ZIRCON GEOCHRONOLOGY OF HUE SHALE STRATA ALONG THE CANNING RIVER, EASTERN NORTH SLOPE, ALASKA

Trystan M. Herriott, James L. Crowley, and Marwan A. Wartes

Raw Data File 2025-24

Photograph of Hue Shale beds at the Emerald Isle section along the Canning River's west bank in northeastern Alaska. Zircon sample 14TMH049-59.5A was collected from the pale yellow and orange-brown bentonite near the blue pencil (14 cm long, for sense of scale) at upper-left.

2025
STATE OF ALASKA
DEPARTMENT OF NATURAL RESOURCES
DIVISION OF GEOLOGICAL & GEOPHYSICAL SURVEYS

STATE OF ALASKA
Mike Dunleavy, Governor

DEPARTMENT OF NATURAL RESOURCES
John Boyle, Commissioner

DIVISION OF GEOLOGICAL & GEOPHYSICAL SURVEYS
Erin A. Campbell, State Geologist & Director

Publications produced by the Division of Geological & Geophysical Surveys are available to download from the DGGS website (dggs.alaska.gov). Publications on hard-copy or digital media can be examined or purchased in the Fairbanks office:

Alaska Division of Geological & Geophysical Surveys (DGGS)
3354 College Road | Fairbanks, Alaska 99709-3707
Phone: 907.451.5010 | Fax 907.451.5050
dggspubs@alaska.gov | dggs.alaska.gov

DGGS publications are also available at:

Alaska State Library, Historical
Collections & Talking Book Center
395 Whittier Street
Juneau, Alaska 99801

Alaska Resource Library and
Information Services (ARLIS)
3150 C Street, Suite 100
Anchorage, Alaska 99503

Suggested citation:
Herriott, T.M., Crowley, J.L., and Wartes, M.A., 2025, Zircon geochronology of Hue Shale strata along the Canning River, eastern North Slope, Alaska: Alaska Division of Geological & Geophysical Surveys Raw Data File 2025-24, 13 p. https://doi.org/10.14509/31728

ZIRCON GEOCHRONOLOGY OF HUE SHALE STRATA ALONG THE CANNING RIVER, EASTERN NORTH SLOPE, ALASKA

Trystan M. Herriott[1], James L. Crowley[2], and Marwan A. Wartes[1]

INTRODUCTION

This Alaska Division of Geological & Geophysical Surveys (DGGS) Raw Data File presents laser ablation-inductively coupled plasma mass spectrometry (LA-ICPMS) and paired chemical abrasion-isotope dilution-thermal ionization mass spectrometry (CA-ID-TIMS) U–Pb results for two zircon samples collected from an exposure along the west bank of the Canning River known as Emerald Island (Macquaker and others, 1999) or Emerald Isle (Lease and others, in revision; fig. 1). The samples are from bentonitic beds in a distal, condensed, deep-water succession of

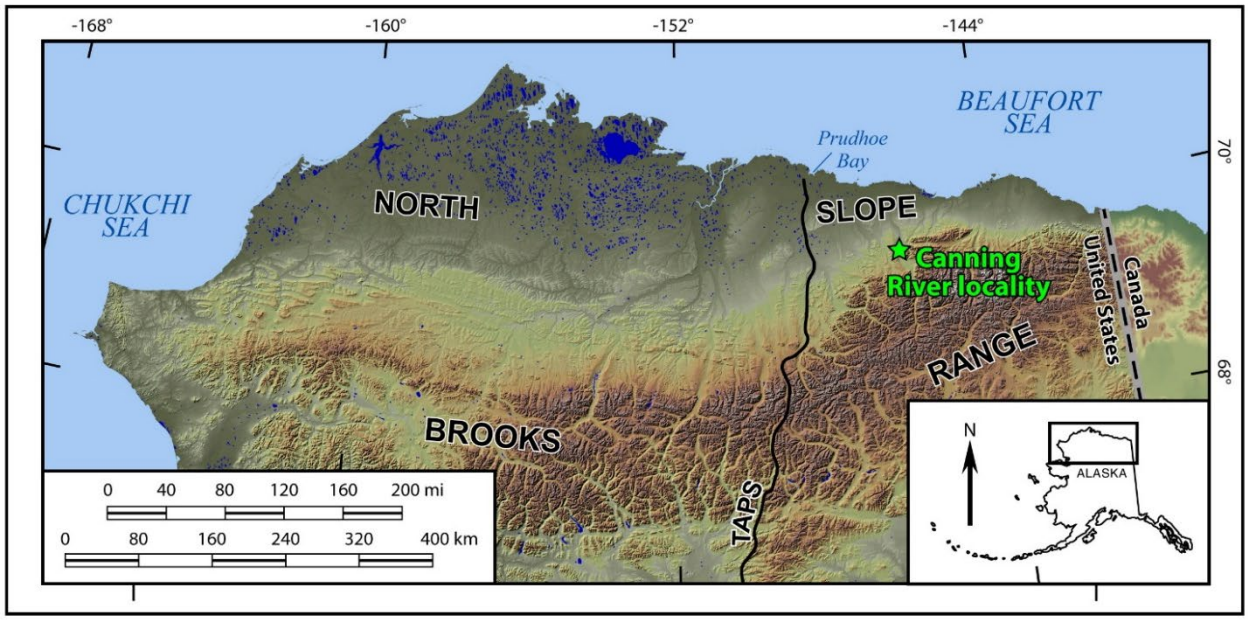

Figure 1. Northern Alaska location map, which highlights the Canning River sample locality known as Emerald Isle (Lease and others, in revision). See text for sample location coordinates. Abbreviation: TAPS: Trans-Alaska Pipeline System.

Cretaceous Hue Shale (Molenaar and others, 1987) in the Colville foreland basin (Bird and Houseknecht, 2011; Houseknecht, 2019). The lower sample is from near the base of the foreland basin sequence in the gamma ray zone (also known as the highly radioactive zone), and the upper sample is from the *Inoceramus* zone (Bird and Molenaar, 1987; Lease and others, 2024, and in revision). The samples were collected in 2014 in support of DGGS's long-running North Slope basin analysis and petroleum systems program and later analyzed as part of our high-precision,

[1]Alaska Division of Geological & Geophysical Surveys, 3354 College Road, Fairbanks, Alaska 99709
[2]Department of Geosciences, Boise State University, 1910 University Drive, Boise, Idaho 83725

zircon-based chronostratigraphy research efforts (see Herriott and others, 2019, 2024, 2025). This data release serves as the permanent, publicly accessible archive for these U–Pb zircon results. A chronostratigraphic interpretation of the Emerald Isle section, including the high-precision zircon ages reported here, is presented in the pending paper by Lease and others (in revision).

LIST OF DELIVERABLES

- This Raw Data File report includes:
  - **Appendix A.** Detailed U–Pb zircon geochronology methods for LA-ICPMS and CA-ID-TIMS.
  - **Appendix B.** Cathodoluminescence images of zircon analyzed during this study. Laser ablation spot locations (red circles) and analysis numbers (white labels) are included. CA-ID-TIMS analysis designations and dates and analytical uncertainties (2σ) are also noted (orange labels).
- Accompanying digital data comprises:
  - **Data File 1.** LA-ICPMS U–Pb geochronology results and related data. Each file includes instrumental data, sample data, standard data, and data dictionary worksheets.
    - A. Hue Shale (*Inoceramus* zone), zircon sample 14TMH049-59.5A.
    - B. Hue Shale (gamma ray zone/highly radioactive zone), zircon sample 14TMH049-28.5A.
  - **Data File 2.** CA-ID-TIMS U–Pb zircon geochronology data for Hue Shale zircon samples 14TMH049-59.5A and 14TMH049-28.5A. A data dictionary worksheet is also included.
  - **Data File 3.** Summary of interpreted CA-ID-TIMS ages in a geodatabase-ready format (A) and a data dictionary (B).
  - **Data File 4.** Summaries of the U–Pb zircon geochronology data in machine-readable formats.
    - A. LA-ICPMS data.
    - B. Data dictionary for A.
    - C. CA-ID-TIMS data.
    - D. Data dictionary for C.

All files associated with this report are available for download on the DGGS website at https://doi.org/10.14509/31728.

SAMPLES

Zircon samples were collected from bentonite-bearing beds of the Hue Shale, using typical field sampling protocols and taking great care to avoid contamination. The reported WGS84 latitude and longitude sample locations are based on an outcrop photograph and satellite imagery analysis.

Descriptions (descending stratigraphic order)

*14TMH049-59.5A: Hue Shale (*Inoceramus *zone)*

Pale yellow (weathering) and orange-brown (fresh), ~8–10-cm-thick bentonite. Stratigraphic height of the sample is correlated to 62.0 m of Lease and others (in revision), which is 34.0 m above the pebble shale unit and 62.0 m above the Kemik Sandstone (see van der Kolk [2010], van der Kolk and others [2015], and Wartes and others [2011] for stratigraphic unit relations). The sample was collected ~2 m above the faulted base of the *Inoceramus* zone, which is ~7 m thick (as exposed) at the sampled section; this thickness is comparable to the *Inoceramus* zone at Hue Creek (Lease and others, in revision) and regional thicknesses of 6–8 m reported by Bird and Molenaar (1987). Sample location coordinates are 69.52990°N 146.30314°W (WGS84).

14TMH049-28.5A: Hue Shale (gamma ray zone/highly radioactive zone)

Dark gray to medium gray-grown, bentonite-bearing mudstone. Stratigraphic height of the sample is correlated to 29.5 m of Lease and others (in revision), which is 1.5 m above the pebble shale unit and 29.5 m above the Kemik Sandstone. Sample location coordinates are 69.52962°N 146.30330°W (WGS84).

METHODS OVERVIEW

Zircon grains from the two Canning River samples were separated and analyzed by U–Pb geochronology at the Boise State University Isotope Geology Laboratory. All samples were analyzed first by LA-ICPMS, delineating the overall character of date distributions and distinguishing approximately syn-eruptive versus clearly xenocrystic or otherwise older zircon. Six zircon crystals from each sample were plucked from their epoxy mounts for analysis by CA-ID-TIMS; follow-up selection criteria typically included LA-ICPMS data, zoning character, grain morphology (for example, favoring sharply faceted crystals consistent with air-fall origin), and presence of melt inclusions suggestive of late-stage, rapid crystallization. Appendix A provides detailed analytical methods for the LA-ICPMS and CA-ID-TIMS experiments. Appendix B presents cathodoluminescence images of zircon analyzed during this study, including annotations as noted above.

RESULTS

The Hue Shale sample results are consistent with tephra deposits, with bentonite being the alteration product of volcanic air-fall material that settled through the water column and accumulated on the deep-water basin floor. Depositional ages are established by calculating a weighted mean of the CA-ID-TIMS dates that overlap at ± 2σ analytical uncertainty and yield a probability of fit >0.05. All dates and ages noted below are $^{206}Pb/^{238}U$; see appendix A for an

explanation of X (Y) [Z] levels of uncertainty for CA-ID-TIMS results. Data files 1–4 include complete data tables, results summaries, and supporting metadata.

Forty-four zircon grains from 14TMH049-59.5A analyzed by LA-ICPMS yielded nearly entirely (n = 43 of 44) mid-Cretaceous dates of ~89–109 Ma; one Triassic date (~229 Ma) was obtained. Six grains were analyzed by CA-ID-TIMS, with three dates yielding a weighted mean age of 95.762 ± 0.040 (0.049) [0.114] Ma at 2σ (MSWD = 0.61, probability of fit = 0.54; data files 2 and 3). Three slightly older CA-ID-TIMS dates are 96.058 ± 0.069 Ma, 96.315 ± 0.066 Ma, and 96.325 ± 0.082 Ma (data file 2).

Fifty-five zircon grains from 14TMH049-28.5A analyzed by LA-ICPMS yielded nearly entirely (n = 54 of 55) Early Cretaceous dates of ~110–129 Ma; one Permian date (~285 Ma) was obtained. Six grains were analyzed by CA-ID-TIMS, with all 6 dates yielding a weighted mean age of 115.700 ± 0.032 (0.047) [0.133] Ma at 2σ (MSWD = 1.60, probability of fit = 0.16; data files 2 and 3).

ACKNOWLEDGMENTS

The State of Alaska funded this study, and funding for the analytical infrastructure of the Boise State University Isotope Geology Laboratory (BSUIGL) is provided by the National Science Foundation (grants EAR-0521221, EAR-0824974, EAR-1337887, EAR-1735889, and EAR-1920336 awarded to Mark D. Schmitz and others). We thank Dr. Schmitz for supporting the DGGS–BSUIGL collaboration; we also thank BSUIGL staff for their assistance. Discussions with Richard Lease and William Rouse provided additional stratigraphic context for the Canning River samples.

REFERENCES

Bird, K.J., and Houseknecht, D.W., 2011, Geology and petroleum potential of the Arctic Alaska petroleum province, in Spencer, A.M., Embry, A.F., Gautier, D.L., Stoupakova, A.V., and Sørensen, K., eds., Arctic petroleum geology: Geological Society of London Memoir 35, ch. 32, p. 485–499, https://doi.org/10.1144/M35.32

Bird, K.J., and Molenaar, C.M., 1987, Stratigraphy, in Bird, K.J., and Magoon, L.B., eds., Petroleum geology of the northern part of the Arctic National Wildlife Refuge, northeastern Alaska: U.S. Geological Survey Bulletin 1778, p. 37–59, https://doi.org/10.3133/b1778

Herriott, T.M., Crowley, J.L., LePain, D.L., Wartes, M.A., Harun, N.T., and Schmitz, M.D., 2024, Zircon geochronology of Torok and Nanushuk Formations sandstones at Slope Mountain and a Seabee Formation tephra deposit at Ninuluk Bluff, central North Slope, Alaska: Alaska Division of Geological & Geophysical Surveys Raw Data File 2024-33, 22 p., https://doi.org/10.14509/31152

Herriott, T.M., Crowley, J.L., Schmitz, M.D., Wartes, M.A., and Gillis, R.J., 2019, Exploring the law of detrital zircon: LA-ICP-MS and CA-TIMS geochronology of Jurassic forearc strata, Cook Inlet, Alaska, USA: Geology, v. 47, p. 1044–1048, https://doi.org/10.1130/G46312.1

Herriott, T.M., Crowley, J.L., Wartes, M.A., LePain, D.L., and Schmitz, M.D., 2025 (in press), Accuracy and validity of maximum depositional ages in light of tandem (laser ablation and isotope dilution) U–Pb detrital zircon geochronology, including results from northern Alaska: Geochronology

Houseknecht, D.W., 2019, Evolution of the Arctic Alaska sedimentary basin, in Miall, A.D., ed., The sedimentary basins of the United States and Canada, 2nd ed.: Elsevier, ch. 18, p. 719–745, https://doi.org/10.1016/B978-0-444-63895-3.00018-8

Lease, R.O., Whidden, K.J., Dumoulin, J.A., Houseknecht, D.W., Botterell, P.J., Dreier, M.F., Griffis, N.P., Mundil, R., Kylander-Clark, A.R.C., Sanders, M.M., Counts, J.W., Self-Trail, J.M., Gooley, J.T., Rouse, W.A., Smith, R.A., and DeVera, C.A., 2024, Arctic Alaska deepwater organic carbon burial and environmental changes during the late Albian–early Campanian (103–82 Ma): Earth and Planetary Science Letters, v. 646, 118948, 9 p., https://doi.org/10.1016/j.epsl.2024.118948

Lease, R.O., Whidden, K.J., Dumoulin, J.A., Houseknecht, D.W., Kylander-Clark, A.R.C., Harper, J., Herriott, T.M., and Gooley, J.T., in revision, Regional 116–68 Ma ash zircon U–Pb dates from Arctic Alaska deepwater strata and a carbon isotopic framework for Oceanic Anoxic Events 1d, 2, 3a, 3b, and 3c: Geological Society of London Special Publications

Macquaker, J.H.S., Keller, M.A., and Taylor, K.G., 1999, Sequence stratigraphic analysis of the lower part of the pebble shale unit, Canning River, northeastern Alaska, in ANWR Assessment Team, The oil and gas resource potential of the 1002 Area, Arctic National Wildlife Refuge, Alaska: U.S. Geological Survey Open-File Report 98-34, p. SS-1–SS-28, https://doi.org/10.3133/ofr9834

Molenaar, C.M., Bird, K.J., and Kirk, A.R., 1987, Cretaceous and Tertiary stratigraphy of northeastern Alaska, in Tailleur, I.L., and Weimer, P., eds., Alaskan North Slope geology: Society of Economic Paleontologists and Mineralogists (SEPM), Pacific Section, and Alaska Geological Society, Book 50, v. 1, p. 513–528

van der Kolk, D.A., 2010, Geochemistry, sedimentology, and stratigraphy of the Lower Cretaceous pebble shale unit, northeastern Alaska: University of Alaska Fairbanks, M.S. thesis, 116 p., 1 plate

van der Kolk, D.A., Whalen, M.T., and Wartes, M.A., 2015, Source-rock potential of the Lower Cretaceous pebble shale unit, northeastern Alaska: Alaska Division of Geological & Geophysical Surveys Preliminary Interpretive Report 2015-1, 37 p., https://doi.org/10.14509/29401

Wartes, M.A., Wallace, W.K., Loveland, A.M., Gillis, R.J., Decker, P.L., Reifenstuhl, R.R., Delaney, P.R., LePain, D.L., and Carson, E.C., 2011, Geologic map of the Kavik River area, northeastern Brooks Range, Alaska: Alaska Division of Geological & Geophysical Surveys Report of Investigation 2011-3A, 14 p., 1 sheet, scale 1:63,360, https://doi.org/10.14509/22602

APPENDIX A. DETAILED U–PB ZIRCON GEOCHRONOLOGY METHODS

Laser Ablation-Inductively Coupled Plasma Mass Spectrometry

Zircon grains were separated from rocks using standard techniques, annealed at 900°C for 60 hours in a muffle furnace, and mounted in epoxy and polished until their centers were exposed. Cathodoluminescence (CL) images (appendix B) were obtained with a Hitachi TM4000Plus scanning electron microscope. Zircon was analyzed by laser ablation-inductively coupled plasma mass spectrometry (LA-ICPMS) using an iCAP RQ Quadrupole ICPMS and Teledyne Photon Machines Analyte Excite+ 193 nm excimer laser ablation system with HelEx II Active two-volume ablation cell. In-house analytical protocols, standard materials, and data reduction software were used for acquisition and calibration of U–Pb dates and a suite of high field strength elements and rare earth elements. Zircon was ablated with a laser spot of 20 μm wide using fluence and pulse rates of 2.5 J/cm^2 and 10 Hz, respectively, during a 25-second analysis (15-second gas blank, 10-second ablation) that excavated a pit ~8 μm deep. Ablated material was carried by a 0.25 L/min He gas stream in the inner cell and a 1.25 L/min He gas stream in the outer cell. Dwell times and other instrumental data are given in the "Instrumental data" worksheets of data file 1. Background count rates for each analyte were obtained prior to each spot analysis and subtracted from the raw count rate for each analyte. Ablations pits that appear to have intersected glass or mineral inclusions were identified based on Ti and P. U–Pb dates from these analyses are considered valid if the U–Pb ratios appear to have been unaffected by the inclusions. Analyses that appear contaminated by common Pb were rejected based on mass 204 being above baseline. For concentration calculations, background-subtracted count rates for each analyte were internally normalized to ^{29}Si and calibrated with respect to NIST SRM-610 and -612 glasses as the primary standards. Temperature was calculated from the Ti-in-zircon thermometer (Watson and others, 2006). Because there are no constraints on the activity of TiO_2, an average value in crustal rocks of 0.6 was used.

For U-Pb and ^{207}Pb/^{206}Pb dates, instrumental fractionation of the background-subtracted ratios was corrected and dates were calibrated with respect to interspersed measurements of zircon standards and reference materials. The primary standard Plešovice zircon (Sláma and others, 2008) was used to monitor time-dependent instrumental fractionation based on two analyses for every 12 analyses of unknown zircon. A secondary correction to the ^{206}Pb/^{238}U dates was made based on results from the zircon standards Seiland (531 Ma, Kuiper and others, 2022) and 91500 (1065 Ma, Wiedenbeck and others, 1995), which were treated as unknowns and measured once for every 12 analyses of unknown zircon. These results (see "Standard data" worksheets of data file 1) showed a linear age bias of several percent that is related to the ^{206}Pb count rate. The secondary correction is thought to mitigate matrix-dependent variations due to contrasting compositions and ablation characteristics between the Plešovice zircon and other standards (and unknowns).

Radiogenic isotope ratio and age error propagation for all analyses includes uncertainty contributions from counting statistics and background subtraction. Errors without and with the standard calibration uncertainty are shown in the "Sample data" worksheets of data file 1. This uncertainty is the local standard deviation of the polynomial fit to the interspersed primary

standard measurements versus time for the time-dependent, relatively larger U/Pb fractionation factor, and the standard error of the mean of the consistently time-invariant and smaller $^{207}Pb/^{206}Pb$ fractionation factor. These uncertainties are given in the "Instrumental data" worksheets of data file 1. A standard calibration uncertainty is then propagated into the error on the date. Discordance is calculated as the relative difference between $^{207}Pb/^{235}U$ and $^{206}Pb/^{238}U$ dates; unless otherwise noted on "Instrumental data" worksheets of data file 1, analyses with discordance outside of uncertainty of 5% are formatted with strike-through and placed at the bottom of the "Sample data" worksheets of data file 1. Errors are at 2σ.

Chemical Abrasion-Isotope Dilution Thermal Ionization Mass Spectrometry

U–Pb dates were obtained by the chemical abrasion-isotope dilution-thermal ionization mass spectrometry (CA-ID-TIMS) method from analyses composed of single zircon grains (data file 2), modified after Mattinson (2005). Zircon was removed from the epoxy mounts for isotope dilution dating based on LA-ICPMS data (data file 1) and CL imagery (appendix B).

Zircon was loaded into 300 µl Teflon PFA microcapsules, placed in a large-capacity Parr vessel, and partially dissolved in 120 µl of 29 M HF for 12 hours at 190°C. Contents of the microcapsules were then put in 3 ml Teflon PFA beakers, the HF was removed, and zircon was then immersed in 3.5 M HNO_3, ultrasonically cleaned for 30 minutes, and fluxed on a hotplate at 80°C for an hour. The HNO_3 was removed, and zircon was rinsed twice in ultrapure H_2O before being reloaded into the 300 µl Teflon PFA microcapsules (rinsed and fluxed in 6 M HCl for several hours) and spiked with the EARTHTIME mixed ^{233}U-^{235}U-^{205}Pb tracer solution (ET535, Condon and others, 2015). Zircon was dissolved in Parr vessels in 120 µl of 29 M HF at 220°C for 48 hours, dried to fluorides, and re-dissolved in 6 M HCl at 180°C overnight. U and Pb were separated from the zircon matrix using an HCl-based anion-exchange chromatographic procedure (Krogh, 1973), eluted together, and dried with 2 µl of 0.05 N H_3PO_4.

Pb and U were loaded on a single outgassed Re filament in 5 µl of a silica-gel/phosphoric acid mixture (Gerstenberger and Haase, 1997), and U and Pb isotopic measurements were made on a GV Isoprobe-T multicollector thermal ionization mass spectrometer equipped with an ion-counting Daly detector. Pb isotopes were measured by peak-jumping all isotopes on the Daly detector for 160–220 cycles and corrected for 0.16 ± 0.03%/a.m.u. (1σ) mass fractionation. Transitory isobaric interferences due to high-molecular weight organics, particularly on ^{204}Pb and ^{207}Pb, disappeared within approximately 60 cycles, while ionization efficiency averaged 10^4 cps/pg of each Pb isotope. Linearity (to ≥1.4 x 10^6 cps) and the associated deadtime correction of the Daly detector were determined by analysis of NBS982. U was analyzed as UO_2^+ ions in static Faraday mode on 10^{12} ohm resistors for 300 cycles and corrected for isobaric interference of $^{233}U^{18}O^{16}O$ on $^{235}U^{16}O^{16}O$ with an $^{18}O/^{16}O$ of 0.00206. Ionization efficiency averaged 20 mV/ng of each U isotope. U mass fractionation was corrected using the known $^{233}U/^{235}U$ ratio of the ET535 tracer solution.

U–Pb dates and uncertainties were calculated using the algorithms of Schmitz and Schoene (2007), ET535 tracer solution (Condon and others, 2015) with calibration of $^{235}U/^{205}Pb$ = 100.233,

$^{233}U/^{235}U$ = 0.99506, and $^{205}Pb/^{204}Pb$ = 11268, and U decay constants recommended by Jaffey and others (1971) and $^{238}U/^{235}U$ of 137.818 (Hiess and others, 2012). $^{206}Pb/^{238}U$ ratios and dates were corrected for initial ^{230}Th disequilibrium using $D_{Th/U} = 0.2 \pm 0.1$ (2σ) and the algorithms of Crowley and others (2007), increasing the $^{206}Pb/^{238}U$ dates by ~0.09 Ma. All common Pb in analyses was attributed to laboratory blank and subtracted based on the measured laboratory Pb isotopic composition and associated uncertainty. U blanks are estimated at 0.013 pg.

Weighted mean $^{206}Pb/^{238}U$ and $^{207}Pb/^{206}Pb$ dates are calculated from equivalent dates (probability of fit >0.05) using Isoplot 3.0 (Ludwig, 2003); errors at the 95% confidence interval and 2σ are reported in data file 2. For 95% confidence interval, error is computed as the internal standard deviation multiplied by the Student's t-distribution multiplier for a two-tailed 95% critical interval and n–1 degrees of freedom when the reduced chi-squared statistic, mean squared weighted deviation (MSWD) (Wendt and Carl, 1991), takes a value less than its expectation value plus its standard deviation at the same confidence interval, which is when MSWD is <1+2*sqrt[2/(n–1)]. This error is expanded via multiplication by the sqrt(MSWD) when the MSWD is ≥1+2*sqrt[2/(n–1)] to accommodate unknown sources of overdispersion. Errors on weighted mean ages are $^{206}Pb/^{238}U$ interpreted ages are given as ± X (Y) [Z], where X is the internal error based on analytical uncertainties only, including counting statistics, subtraction of tracer solution, and blank Pb subtraction; Y includes the tracer calibration uncertainty propagated in quadrature; and Z includes the ^{238}U decay constant uncertainty propagated in quadrature. Internal errors (X) should be considered when comparing our dates with $^{206}Pb/^{238}U$ CA-ID-TIMS dates from other laboratories that used the same tracer solution or a tracer solution that was cross-calibrated using EARTHTIME gravimetric standards. Errors including the uncertainty in the tracer calibration (Y) should be considered when comparing our dates with those derived from other geochronological methods using the U–Pb decay scheme (for example, LA-ICPMS). Errors including uncertainties in the tracer calibration and ^{238}U decay constant (Jaffey and others, 1971) (Z) should be considered when comparing our dates with those derived from other decay schemes (for example, $^{40}Ar/^{39}Ar$, $^{187}Re–^{187}Os$). Errors on dates from individual analyses are 2σ.

Appendix A References

Condon, D.J., Schoene, B., McLean, N.M., Bowring, S.A., and Parrish, R.R., 2015, Metrology and traceability of U–Pb isotope dilution geochronology (EARTHTIME Tracer Calibration Part I): Geochimica et Cosmochimica Acta, v. 164, p. 464–480, https://doi.org/10.1016/j.gca.2015.05.026

Crowley, J.L., Schoene, B., and Bowring, S.A., 2007, U–Pb dating of zircon in the Bishop Tuff at the millennial scale: Geology, v. 35, p. 1123–1126, https://doi.org/10.1130/G24017A.1

Gerstenberger, H., and Haase, G., 1997, A highly effective emitter substance for mass spectrometric Pb isotope ratio determinations: Chemical Geology, v. 136, p. 309–312, https://doi.org/10.1016/S0009-2541(96)00033-2

Hiess, J., Condon, D.J., McLean, N., and Noble, S.R., 2012, 238U/235U systematics in terrestrial uranium-bearing minerals: Science, v. 335, p. 1610–1614, https://doi.org/10.1126/science.1215507

Jaffey, A.H., Flynn, K.F., Glendenin, L.E., Bentley, W.C., and Essling, A.M., 1971, Precision measurements of half-lives and specific activities of 235U and 238U: Physical Review C, v. 4, p. 1889–1906

Krogh, T.E., 1973, A low-contamination method for hydrothermal decomposition of zircon and extraction of U and Pb for isotopic age determination: Geochimica et Cosmochimica Acta, v. 37, p. 485–494, https://doi.org/10.1016/0016-7037(73)90213-5

Kuiper, Y.D., Murray, D.P., Ellison, S., and Crowley, J.L., 2022, U–Pb detrital zircon analysis of sedimentary rocks of the southeastern New England Avalon terrane in the U.S. Appalachians: Evidence for a separate crustal block, in Kuiper, Y.D., Murphy, J.B., Nance, R.D., Strachan, R.A., and Thompson, M.D., eds., New Developments in the Appalachian-Caledonian-Variscan Orogen: Geological Society of America Special Paper 554, p. 93–119, https://doi.org/10.1130/2021.2554(05)

Ludwig, K.R., 2003, User's Manual for Isoplot 3.00: Berkeley Geochronology Center, Berkeley, California, 70 p.

Mattinson, J.M., 2005, Zircon U–Pb chemical abrasion ("CA-TIMS") method: Combined annealing and multi-step partial dissolution analysis for improved precision and accuracy of zircon ages: Chemical Geology, v. 220, p. 47–66, https://doi.org/10.1016/j.chemgeo.2005.03.011

Schmitz, M.D., and Schoene, B., 2007, Derivation of isotope ratios, errors, and error correlations for U–Pb geochronology using 205Pb-235U-(233U)-spiked isotope dilution thermal ionization mass spectrometric data: Geochemistry, Geophysics, Geosystems, Q08006, https://doi.org/10.1029/2006GC001492

Sláma, J., Košler, J., Condon, D.J., Crowley, J.L., Gerdes, A., Hanchar, J.M., Horstwood, M.S.A., Morris, G.A., Nasdala, L., Norberg, N., Schaltegger, U., Schoene, B., Tubrett, M.N., and Whitehouse, M.J., 2008, Plešovice zircon—A new natural reference material for U–Pb and Hf isotopic microanalysis: Chemical Geology, v. 249, p. 1–35, https://doi.org/10.1016/j.chemgeo.2007.11.005

Watson, E.B., Wark, D.A., and Thomas, J.B., 2006, Crystallization thermometers for zircon and rutile: Contributions to Mineralogy and Petrology, v. 151, p. 413–433, https://doi.org/10.1007/s00410-006-0068-5

Wendt, I., and Carl, C., 1991, The statistical distribution of the mean squared weighted deviation: Chemical Geology (Isotope Geoscience Section), v. 86, p. 275–285, https://doi.org/10.1016/0168-9622(91)90010-T

Wiedenbeck, M., Allé, P., Corfu, F., Griffin, W.L., Meier, M., Oberli, F., von Quadt, A., Roddick, J.C., and Spiegel, W., 1995, Three natural zircon standards for U–Th–Pb, Lu–Hf, trace element and REE analyses: Geostandards Newsletter, v. 19, p. 1–23, https://doi.org/10.1111/j.1751-908X.1995.tb00147.x

APPENDIX B. CATHODOLUMINESCENCE IMAGES OF ZIRCON

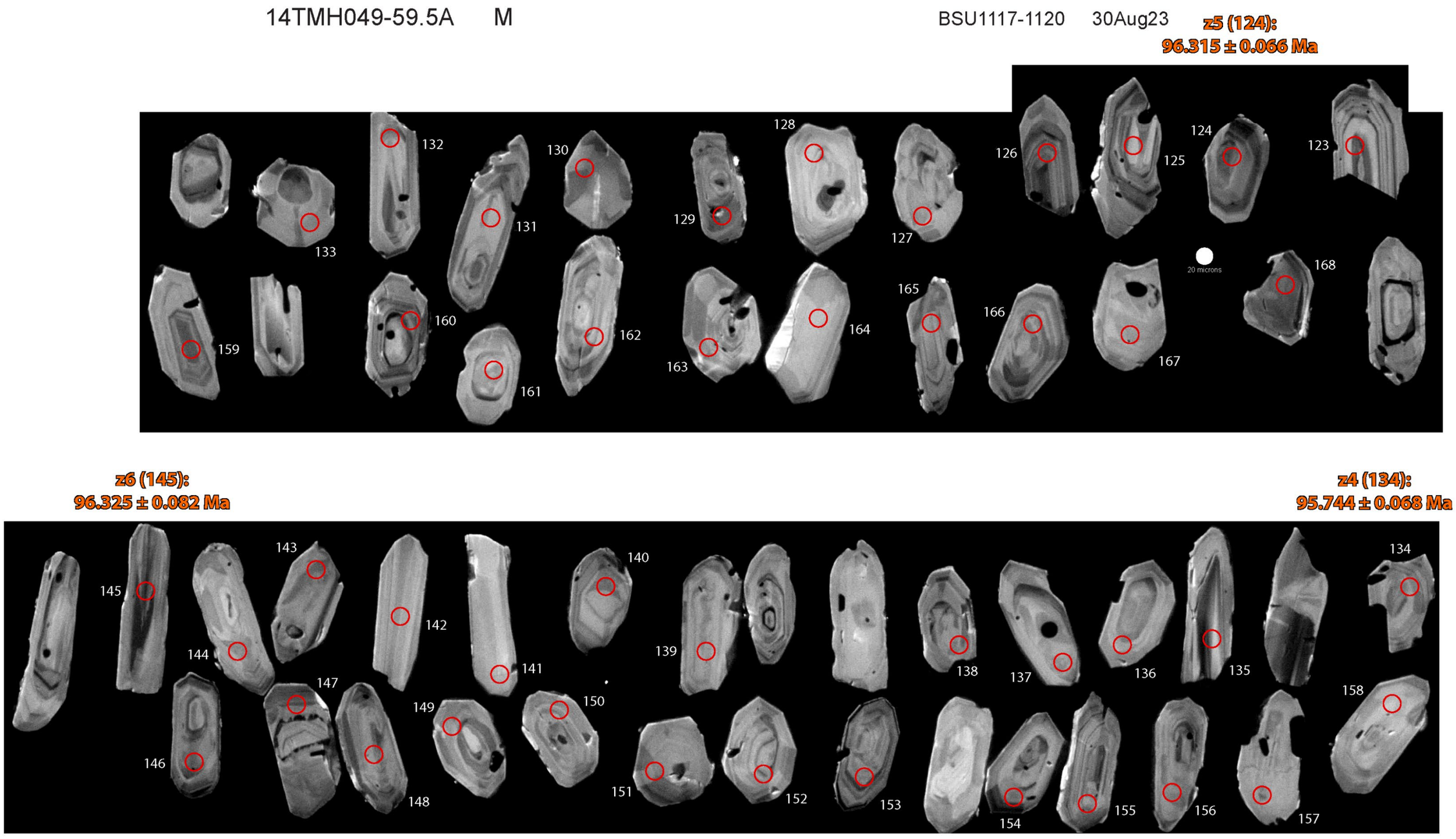

14TMH049-59.5A L BSU1117-1120 30Aug23

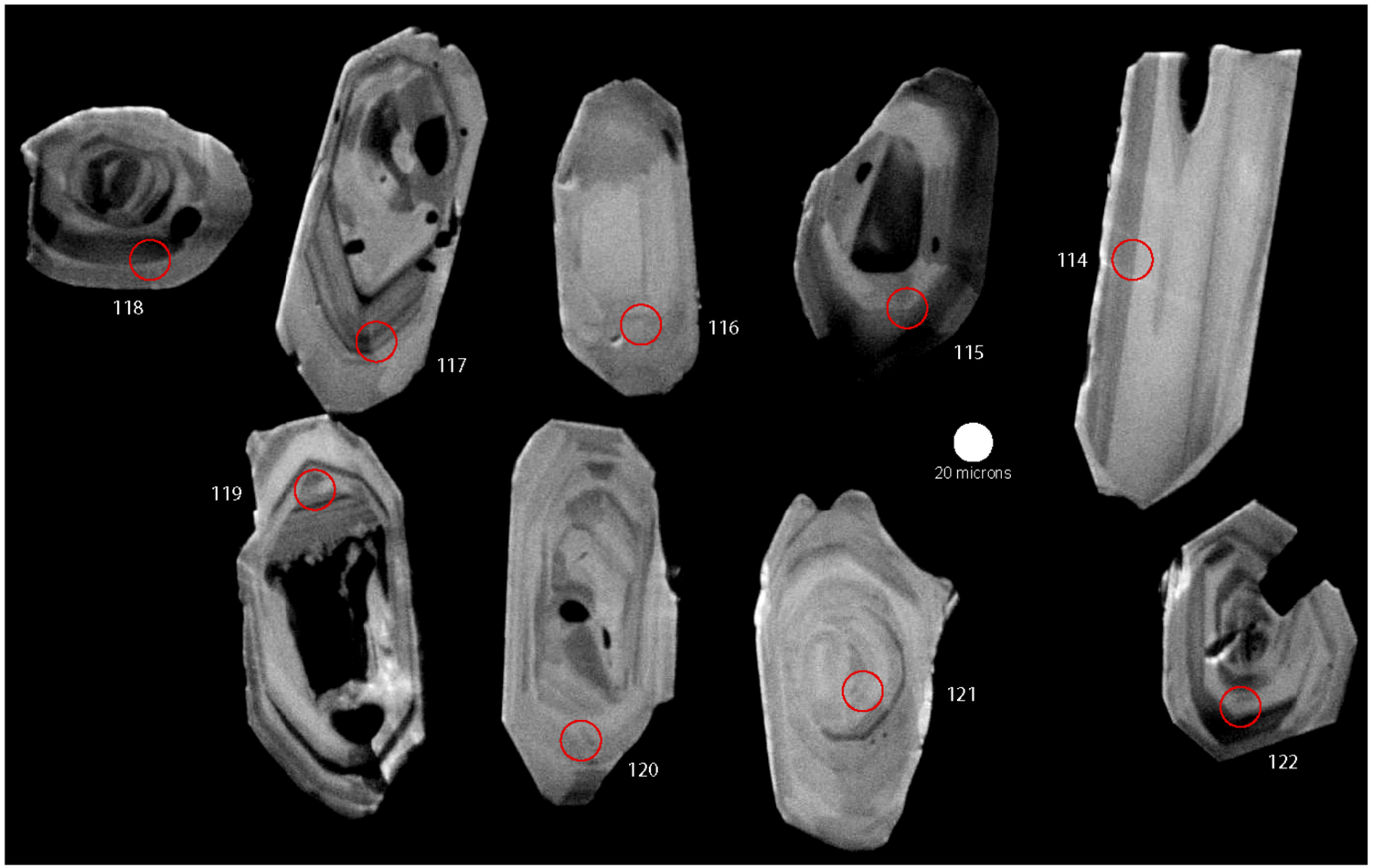

z1 (121): 96.058 ± 0.069 Ma z2 (122): 95.747 ± 0.071 Ma

14TMH049-28.5A S BSU1117-1120 30Aug23

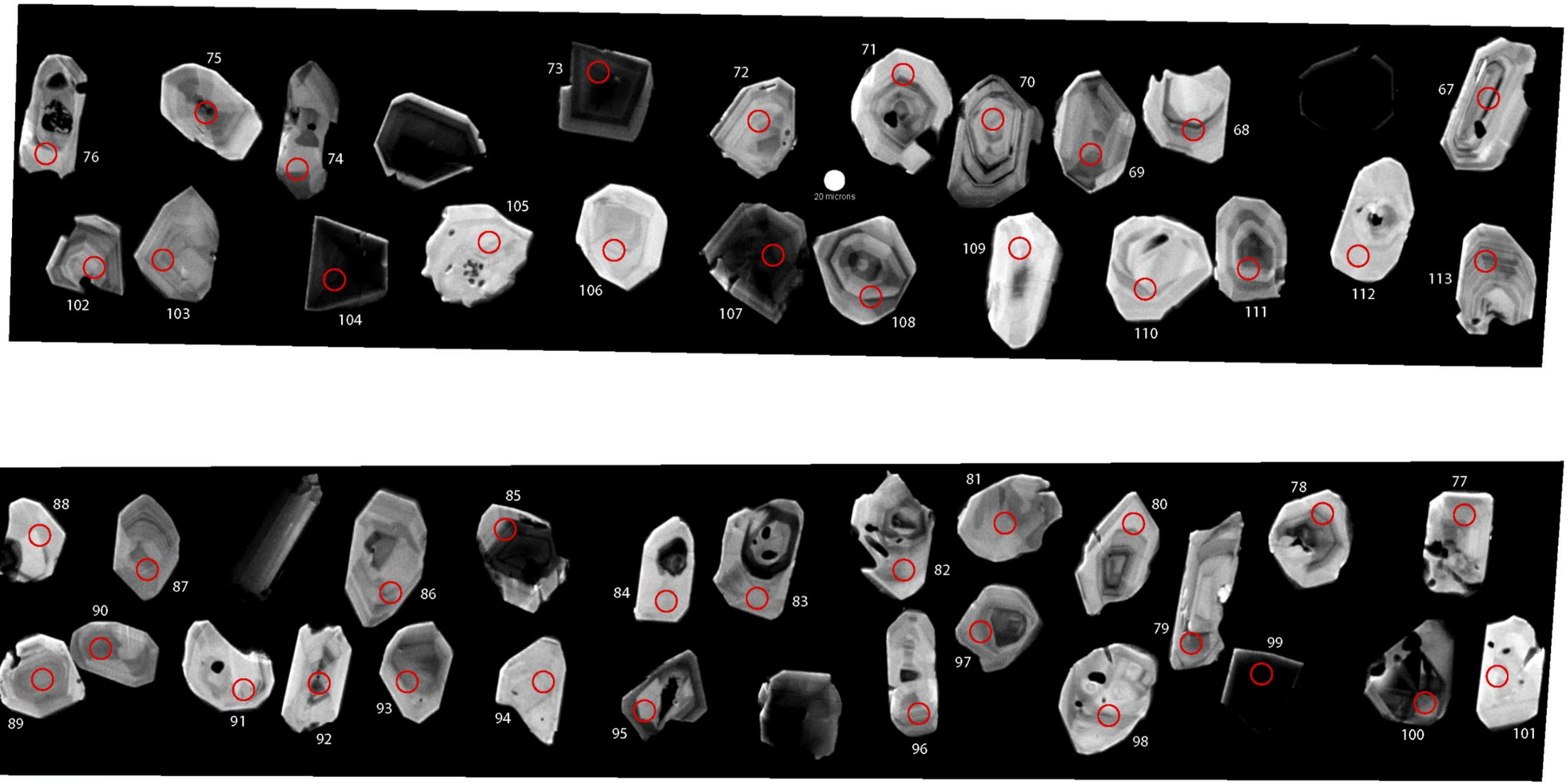

z6 (89):
115.755 ± 0.081 Ma

14TMH049-28.5A M BSU1117-1120 30Aug23

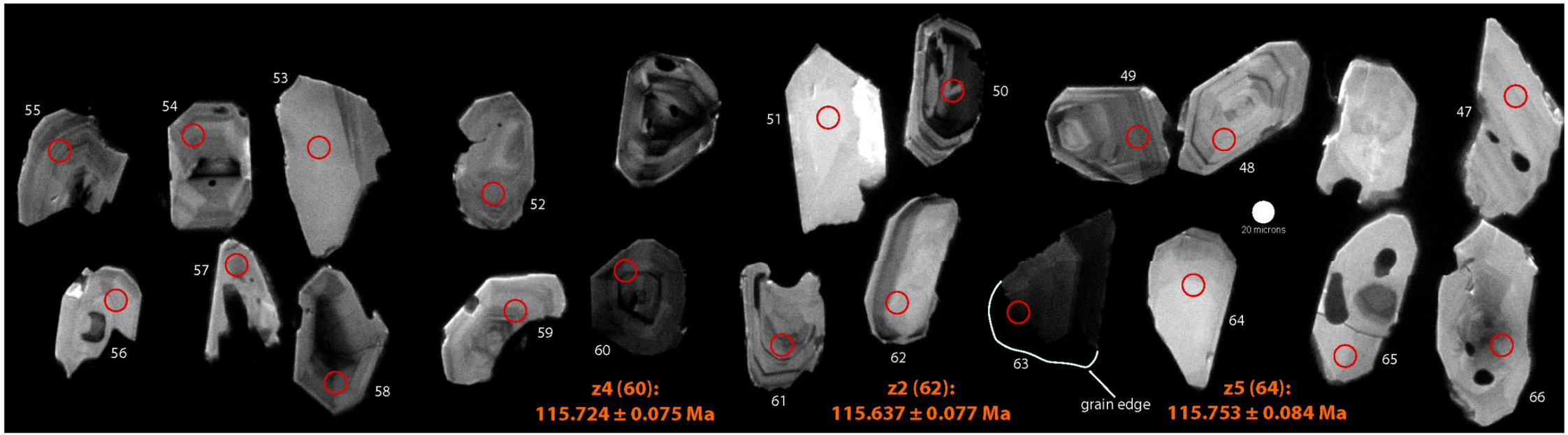

z3 (61):
115.657 ± 0.074 Ma

z1 (63):
115.687 ± 0.077 Ma